PCCP

ROYAL SOCIETY OF CHEMISTRY

PAPER

View Article Online
View Journal | View Issue

Cite this: *Phys. Chem. Chem. Phys.*, 2023, **25**, 8676

Asymmetric Janus functionalization induced magnetization and switchable out-of-plane polarization in 2D MXene Mo_2CXX'†

Chao Xin, *[ab] Zhen Fan,[a] Zhixin Sun,[a] Hui Li,[a] Guangyong Jin,[a] Feng Pan *[b] and Yu Sui*[c]

Received 5th December 2022,
Accepted 27th February 2023

DOI: 10.1039/d2cp05668b

rsc.li/pccp

Exploring two-dimensional (2D) van der Waals materials with out-of-plane polarization and electromagnetic coupling is essential for the development of next-generation nano-memory devices. A novel class of 2D monolayer materials with predicted spin-polarized semi-conductivity, partially compensated antiferromagnetic (AFM) order, fairly high Curie temperature, and out-of-plane polarization is analyzed in this work for the first time. Based on density functional theory calculations, we systematically studied these properties in asymmetrically functionalized MXenes (Janus Mo_2C)-Mo_2CXX' (X, X′ = F, O, and OH). Using *ab initio* molecular dynamics (AIMD) and phonon spectrum calculations, the thermal and dynamic stabilities of six functionalized Mo_2CXX' were identified. Our DFT+*U* calculation results also provided a switching path for out-of-plane polarizations, where the reverse of electric polarization is driven by terminal-layer atom flipping. More importantly, strong coupling between magnetization and electric polarization originating from spin-charge interactions was observed in this system. Our results confirm that Mo_2C-FO would be a novel monolayer electromagnetic material, and its magnetization can be modulated by electric polarization.

1 Introduction

Electromagnetic materials with coupled electric and magnetic orders provide a fantastic opportunity to realize the magnetic control of electric polarization or electrical control of magnetization and are promising materials for fundamental condensed matter physics and high-performance spin electronic devices, such as ultrafast non-volatile electric/magnetic memory devices.[1–4] During the past 20 years, two types of magnetoelectric materials, primarily involving three-dimensional perovskite oxides (*e.g.*, type-I $BiFeO_3$ and type-II Y_2NiMnO_6), have been discovered.[5,6] Inspired by the recent progress in the field of two-dimensional van der Waals (vdW) magnetic and electric materials, increasing efforts have been dedicated to integrating magnetism and electric polarization in 2D vdW materials, which can further enhance field modulation efficiency and data storage density in processing devices.[7] On the one hand, since the initial discovery of hydroxyl-functionalized 2D ferroelectric graphene,[8] several 2D materials, such as SnS,[9] 1T-MoS_2,[10] and 2D monolayer materials decorated with polar groups, have been reported to be ferroelectric.[11,12] Experimentally, out-of-plane electric polarization has been found in 2D few-layer $CuInP_2S_6$,[13] while in-plane electric polarization has been predicted and modulated in atom-thick SnTe.[14] On the other hand, 2D ferromagnetism was also predicted in theory and then confirmed experimentally in the CrI_3 and $CrGeTe_3$ layers.[15,16] Furthermore, some research groups have developed magnetoelectric multiferroic materials by modifying or doping 2D monolayers or heterostructures, such as graphene, black phosphorus, and $LaCl/In_2Se_3$.[17–19] All these discoveries have attracted considerable attention in the field of 2D multiferroic physics.[20,21] The coexistence of magnetization and polarization has rarely been reported in 2D materials due to their inherent mutual exclusion. Low critical temperature and weak magnetoelectric coupling are also some bottlenecks of the application of 2D magnetoelectric materials.

Two-dimensional slabs of transition metal (M) carbides and nitrides (X atoms) named "MXenes" are a rapidly growing family of 2D layer materials because of their extensive potential applications.[22] Numerous studies have demonstrated that MXenes are significant 2D layered materials with a variety of mechanical, chemical, optical, and electronic properties.[23] By utilizing the regulatable properties of MXenes, they have been

[a] *School of Science, Changchun University of Science and Technology, Jilin Key Laboratory of Solid-state Laser Technology and Application, Changchun 130022, China. E-mail: xinchao@pkusz.edu.cn*
[b] *School of Advanced Materials, Peking University Shenzhen Graduate School, Shenzhen 518055, China. E-mail: panfeng@pkusz.edu.cn*
[c] *Department of Physics, Harbin Institute of Technology, Harbin 150001, China. E-mail: suiyu@hit.edu.cn*

† Electronic supplementary information (ESI) available. See DOI: https://doi.org/10.1039/d2cp05668b

used in a wide range of applications from energy storage to water purification and desalination, catalysis, optoelectronic, electronics, communication, electromagnetic interference shielding, topological, magnetic, and photothermal therapy.[24] There are two approaches to producing MXenes by removing the A layer atoms (Al, Si, Ga) from the parent MAX phase and related layered compounds, including wet chemical etching and molten salt etching.[25] Due to the chemical activity of bare MXenes, the exposed surfaces are easily passivated by fluorine, oxygen, and hydroxyl radicals. Functionalized MXenes would be the ideal systems to probe room-temperature 2D multiferroicity and the magnetoelectric coupling effect because (1) there are a large number of opportunities for early transition metals and ligand elements, which offer choices to yield strong magnetism[26] and (2) central inversion symmetry breaking induced by the Janus-functionalized atomic layers may bring out-of-plane polarization and interlayer charge asymmetry.[27] In this context, a type-II multiferroic MXene monolayer, namely $Hf_2VC_2F_2$, in which electric polarization is induced directly from its magnetization, has been predicted in this work.[28] Recently, the H-Co_2CF_2 monolayer MXene was determined to be a room-temperature magnetic/ferroelectric semiconductor.[29] MXene surface functionalization can be manipulated by thermal annealing[30] to induce charge disproportionation and tune the electronic properties. These works motivate our investigation of the effects of asymmetric Janus surface termination on magnetic structure, electric polarization, and electromagnetic coupling.

In this work, using DFT+U calculations, we surprisingly predicted that Janus surface functionalization exerts a positive influence on monolayer Mo_2C by (1) inducing charge disproportionation, which leads to ferrimagnetic order (FiM), and (2) inducing switchable out-of-plane electric polarization. Therefore, monolayer Mo_2C-FO with Janus surface termination is an ideal thick monolayer 2D material with coexisting out-of-plane electric polarization and ferrimagnetism. More importantly, strong magnetoelectric coupling originating from the spin-charge interaction was observed in this system. Our results confirm that Janus Mo_2C-FO would be a novel asymmetric Janus monolayer electromagnetic material, and the magnetization can be modulated by electric polarization. Furthermore, we demonstrate that achieving 2D switchable polarization through surface functionalization does not just work in Mo_2C, and to a certain degree, this can be true for other asymmetric Janus MXenes.

2 Calculation details

The first-principles calculations were performed in the framework of the density functional theory (DFT), as implemented in the Vienna *ab initio* simulation package code.[31,32] The Kohn–Sham equation was solved using the generalized gradient approximation (GGA)[33] with DFT-D2, which is a semiempirical dispersion-correction method, and was employed to correct the van der Waals (vdw) interactions.[34] GGA+U correction was applied to strongly correlate the d orbitals of the Mo atoms.[35] We repeated all calculations for diverse values of the U parameter in the 0–6 eV range and thus made sure our qualitative conclusions are reliable. A plane-wave energy cut-off of 500 eV was used. Structural optimization was carried out using a Monkhorst–Pack[36] $8 \times 8 \times 1$ mesh. All structure parameters were sequentially relaxed in such a way that the Hellmann–Feynman forces were less than 0.01 eV $Å^{-1}$, and the total energy changes converged to below 10^{-5} eV. The conjugate gradient algorithm and quasi-Newton algorithm[37] were used for the optimization of the structure. Spontaneous polarization was calculated using the Berry phase method[38] with a $12 \times 12 \times 1$ k-mesh. A vacuum distance larger than 15 Å was set between adjacent slabs to avoid spurious interactions. In order to determine the ground-state magnetic coupling between the Mo atoms, we used a $2 \times 1 \times 1$ supercell that included four Mo atoms. Spin–orbital coupling (SOC) and noncollinear magnetic order were considered in our calculation to evaluate the DM parameters. The visualization and analysis of the structure, spin density and electron localization function (ELF)[39] were carried out using the VESTA code.[40]

3 Results and discussion

A. Structural and electronic properties

Before calculating the electronic structure and properties, we first tested the coulomb repulsion U value of Mo_2C-FO. The relative energies of the different magnetic structures and magnetic moments at each value of U are listed in Tables S1 and S2 (ESI†). The results show that for 0 eV $\leqslant U \leqslant$ 3 eV, AFM2 possessed the lowest energy. For $3 \leqslant U \leqslant 6$ eV, the AFM1 was stable (in which the spin configurations of FM, AFM1 and AFM2 are defined in the next part). When U = 6 eV, the magnetic moments were closer to the quantized integer magnetic moment (2.94/−2.03, $\sim 3/2\mu_B$). Based on a comparison of the comprehensive band gap, total energy and magnetic moment, we finally determined that U = 6 eV is a reasonable value for the Janus Mo_2C system. Unless otherwise indicated, the reported results are for U = 6 eV. The crystal structure of oxygen–fluorine (O–F)-functionalized MXene is plotted in Fig. 1. Pristine MXene M_2C has a three-layer structure with a trigonal lattice and the space group $P\bar{3}m1$ (No. 164). It is composed of triple layers, with a C atomic layer sandwiched between two Mo layers. The in-plane two Mo atoms of the trigonal lattice of the C atoms are located at the (1/3, 2/3) and (2/3, 1/3) sites, respectively. Usually, the upper and lower surfaces are terminated by F, O, OH, Br, Cl, or H groups depending on the synthesis method. In Fig. 1(a) (top view), we can see the Mo atoms arranged in a hexagonal structure, wherein the Mo atoms in two different layers constitute two triangular sublattices. The terminated surface presents the possibility of modulating the electronic properties of MXenes. As shown in Fig. 1(b), the oxygen/fluorine atoms might be located at three different sites on the surface, namely A, B, and T, on each upper and lower surface. Therefore, there are nine possible combinations for the asymmetric Janus surface, as plotted in Fig. ESI1 (ESI†). For each case, the lattice

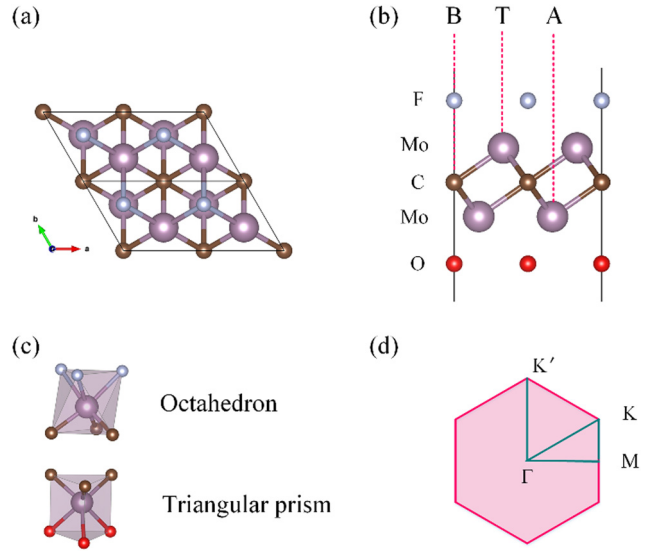

Fig. 1 (a) The top and (b) side views of the Mo_2C-FO MXene lattice. There are three possible sites for X atom decoration on each side of the Janus surface, namely, A (at the hollow position of the Mo atom), B (on top of the C sites), and T (on top of the Mo sites). (c) The distorted octahedron composed of the Mo–C–X atoms, and the triangular prism formed by the O and C ions surrounds Mo. (d) The 2D Brillouin zone integral path.

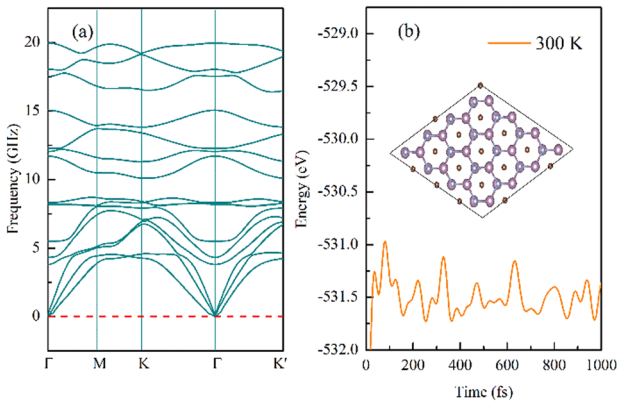

Fig. 2 (a) Variations in the total free energy of Janus Mo_2C-FO during *ab initio* molecular dynamics simulations at 300 K. (b) The phonon spectra of Janus Mo_2C-FO.

parameters and atom positions were fully relaxed by GGA+U, and the structural parameters are listed in Table 1. It can be observed that MXenes with AA-type Janus asymmetry functionalization had the lowest free energy, which is distinguished from the results of HSE.[41] The AA-type structure contains a distorted octahedron composed of Mo–C–X atoms, but in the BB-type structure, the triangular prism formed by the X and C ions surrounds Mo, as seen in Fig. 1(c). Unless otherwise indicated, the reported results are for the AA-type structure. In order to observe the possible spin Rashba split found in Janus MXenes, we extended the 2D Brillouin zone integral path to Γ–M–K–Γ–K', as seen in Fig. 1(d).

The optimized lattice constants in the spin-polarized ground state are listed in Table 1. Due to the asymmetric Janus surface, Mo_2C-F–O, Mo_2C-F-OH, and Mo_2C-O-OH had different layer distances d_1 and d_2, while the symmetric terminal surfaces of Mo_2C-F_2, Mo_2C-O_2, Mo_2C-$(OH)_2$ presented the same layer distances. The asymmetric Janus surface can induce out-of-plane electric polarization, which is discussed below. Mo_2C-F-OH has the largest layer distance d, and Mo_2C-O-OH has the narrowest band gap.

Table 1 The calculated lattice parameters, layer distances (Å), and band gap (eV) of six MXenes

MXenes	a	d_1	d_2	Δd	r	Band gap
Mo_2C-F-O	3.292	2.191	2.395	0.204	3.102	1.1603
Mo_2C-F-OH	3.349	2.319	3.350	1.031	2.985	1.2742
Mo_2C-O-OH	3.242	2.195	3.422	1.227	3.059	0.3632
Mo_2C-F_2	3.349	2.314	2.314	0.000	2.989	2.8846
Mo_2C-O_2	3.245	2.239	2.239	0.000	3.166	0.9576
Mo_2C-$(OH)_2$	3.354	3.342	3.342	0.000	2.994	0.8372

The phonon spectra of the Mo_2CXX' MXenes were calculated using the Phonopy code with the density functional perturbation theory (DFPT) implemented in VASP.[42] Before the DFPT process, we built a 2 × 2 × 1 supercell with Phonopy and then used VASP to optimize the structure. Finally, the phonon spectrums were calculated by using the obtained force constant. The calculated phonon spectra of the six functionalized Mo_2C MXenes are shown in Fig. 2(a) and Fig. ESI2 (ESI†). The unit cell of pristine Mo_2C-FO consisted of 5 atoms, with 15 phonon branches, 3 of which were acoustic (transverse acoustic, longitudinal acoustic, and out-of-plane flexural), whereas the other 12 were optical phonon branches with the absence of imaginary frequencies throughout the Brillouin zone, suggesting that the asymmetric Janus surface and symmetric functionalities of the Mo_2CXX' layer are dynamically stable.

To examine whether the thermodynamics stability and magnetic state of the Mo_2CXX' MXenes are stable at room temperature, we built a large 4 × 4 supercell and performed spin-polarized *ab initio* molecular dynamics (AIMD) simulations with a Nose–Hoover thermostat at 300 K and a time step of 0.5 fs. Fig. 2(b) and Fig. ESI3 (ESI†) display the free energy as a function of the simulation time at 300 K. After 1000 fs, no structural deformation was observed, and the thermal fluctuation range of energy was around ~1 eV, while the equilibration time was ~30 fs, suggesting that the six Mo_2CXX' are thermally stable at room temperature. Most importantly, the system remained magnetic with an average atomic magnetic moment of 3/2 μ_B at 300 K. This demonstrates that the magnetic state of Mo_2CXX' is robust at room temperature. However, the magnetic order may change when the temperature rises, as discussed later with the Monte Carlo simulation results of T_C/T_N.

After considering different types and components that would allow for more realistic models of disorder in Janus asymmetric surface termination, the transition metal oxidation states (determined by the functionalization composition) and the crystal field splitting energy (determined by crystal structural symmetry) were found to most significantly affect the investigated electronic structure and magnetic order. To clearly

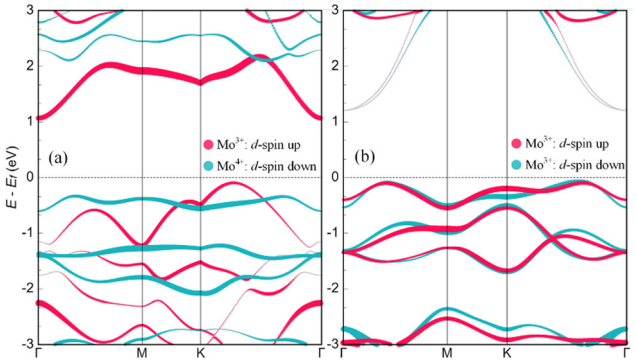

Fig. 3 The spin-polarized d orbital projected band structure of the Mo ions in the six functionalized Mo_2C MXenes: asymmetric Janus (a) Mo_2C-FO and (b) Mo_2C-F-OH; the Fermi level defines zero energy.

demonstrate the spin polarization semiconductor characteristics, we have shown the electronic structures of the Mo_2CXX' monolayer with two spin channels in Fig. 3 and Fig. ESI4 (ESI†). The orbital-resolved features of the energy bands show a predominant contribution of the Mo d orbitals to the dispersing bands near the Fermi level. The HSE06 hybrid functional results calculated by Weng *et al.* show that the ground states of M_2CO_2 and W_2CO_2 are always nonmagnetic. Additionally, MXenes functionalized with oxygen, such as W_2CO_2, are 2D topological insulators exhibiting the largest gap of 0.194 eV.[41] Both Mo_2CO_2 and Cr_2CO_2 show band structures of semimetals with compensated electron and hole Fermi pockets and have the same Z_2 invariant number as W_2CO_2. We tested the band structure of W_2CO_2 and obtained the same topological behavior as Weng *et al.* However, in this work, all the six Mo-basic MXenes showed semiconductor properties with GGA+U (U = 6 eV) solution, as seen in Fig. 3. The band structure results show that the asymmetric Janus terminal atoms driven by internal electric field induce the charge redistribution of Mo. The valence band maximum (VBM) of Mo_2C-FO mainly comprised of 4d orbitals of Mo^{3+} and was located on the K–Γ path in the Brillouin zone. The conduction band minimum (CBM) and VBM of Mo_2C-FOH consist of almost degenerate spin-up and spin-down 4d orbitals of Mo^{3+}. For exploring the possible Rashba spin split, the band structure of Mo_2C-FOH with SOC was also plotted, but we did not observe Rashba splitting. For Mo_2C-OOH (as shown in Fig. ESI4a, ESI†), the VBM comprised the spin-down 4d orbital of Mo^{4+}, while the CBM comprised the spin-up 4d orbital of Mo^{3+}. Additionally, the spin-up and spin-down d orbitals of symmetrically functionalized Mo_2CO_2, Mo_2CF_2, and $Mo_2C(OH)_2$ were degenerated. It had the same characteristics as the one spin channel of Janus MXene. It was also found that the highest valence bands of Mo_2CF_2 and $Mo_2C(OH)_2$ were nearly dispersionless, with a very narrow bandwidth (as shown in Fig. ESI4b and c, ESI†). The charge disproportionation of the Mo ions could be further confirmed by the spin density, as seen in Fig. ESI5 (ESI†). In symmetric surface-decorated Mo_2CX_2, the Mo ions possessed one valence state, for example, Mo^{4+} in Mo_2CO_2 and Mo^{3+} in $Mo_2C(OH)_2$. However, the Mo ions had two valence states in MXenes with Janus asymmetric surface termination, except for Mo_2C-F-OH.

In Mo_2CXX' MXenes, the Mo^{4+} ion had a closed shell Kr core and two remainder 4d electrons, and the Mo^{3+} ion had a closed shell Kr core and three remainder 4d electrons. Pristine Mo_2C and symmetric functionalized Mo_2CO_2, Mo_2CF_2, and $Mo_2C(OH)_2$ had D_{3d} symmetry with the $P3m1$ space group. However, due to the asymmetric Janus surface, mirror inversion symmetry was broken; Mo_2C-FO, Mo_2C-FOH, and Mo_2C-O-OH had C_{3v} symmetry with the $P\bar{3}m1$ space group. Within the C_{3v} symmetry frame of the crystal field, the 4d orbitals of Mo split into two 2-fold degenerate e1 ($d_{x^2-y^2}$ + d_{xy}) and e2 (d_{xz} + d_{yz}) orbitals and a single a (d_{z^2}) orbital. The partial densities of states (PDOS) of Mo^{3+}/Mo^{4+} are plotted in Fig. 4 for the d orbital of the magnetic ions in Mo_2C-FO. The different terminal atoms of the upper and lower surfaces induce the charge disproportionation of the d states in the Mo atoms that have chemically different environments. The competition between on-site Coulomb interactions and crystal field interactions gives rise to the charge disproportionation of Mo ions, which further induces the spin-polarized effect in Janus Mo_2C MXenes.

Another important point is to identify the origin of the antiferromagnetic order of the Mo^{3+} and Mo^{4+} ions. The spin-polarized electron localization functions for Mo_2C-FO are plotted in Fig. 4 inset. The ELF maps show that the Mo atoms near the O layer and F layer ions had distinct d orbitals characteristics. Therefore, the antiferromagnetic coupling between the Mo atoms in Mo_2C-FO is mediated by the C-2p orbitals *via* a

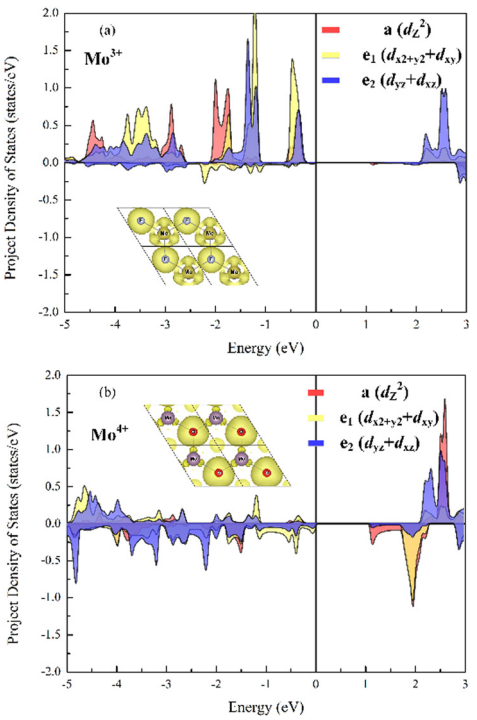

Fig. 4 The projected density of states for the Mn ions in the Mo_2C-FO monolayer: (a) of Mo^{3+}; (b) Mo^{4+}. Inset: Electron localization function (ELF).

double-exchange interaction mechanism.[43] The antiferromagnetic states are more favorable in Mo_2C-FO. Mo_2C-F-OH and Mo_2C-O-OH involve the same AFM coupling mechanism. An analogous AFM magnetic coupling mechanism has been used to reveal the origin of TM-doped 2D materials, cation vacancies in GaN, and 2D TM-dichalcogenides.[44,45] Our calculated electronic properties show that the non-zero magnetization spin-polarized nature is a general feature of Janus asymmetric MXenes, an observation that can lead to the promising application of Janus asymmetry MXenes in spintronics.

B. Monte Carlo simulation of the magnetic transition temperature

The collinear ferromagnetic (FM), type-1 interlayer antiferromagnetic (AFM1), and type-2 intralayer antiferromagnetic (AFM2) states were considered, as shown in Fig. 5(a)–(c). The large exchange splitting ($E_{AFM1} - E_{FM}$) indicates AFM1 was stable in all Mo_2CXX' systems (as shown in Table 2), similar to previously reported results for surface-functionalized Cr_2CT_2.[46] The nearest-(NN) and next-nearest-neighbor exchange (NNN) interactions J_1 and J_2, respectively, defined in Fig. 5(d), were determined by mapping the total energies of the three magnetic structures to a Heisenberg model including the Dzyaloshinskii–Moriya interaction parameter D:

$$\hat{H} = -\sum_{i,j} J_1 S_i \cdot S_j - \sum_{k,l} J_2 S_k \cdot S_l - \sum_i D(S_i)^2$$

where S_i is the net spin at the Mo site i, while (i, j) and (k, l) represent the nearest and next-nearest Mo site pairs, respectively. By mapping the total energies to the Heisenberg model, the exchange interaction J_1 and J_2 were obtained using the following equations:

$$E_{FM} = -6J_1S_1{\cdot}S_2 - 12J_2S_1{\cdot}S_2$$

$$E_{AFM1} = -6J_1S_1{\cdot}S_2 - 12J_2S_1{\cdot}S_2$$

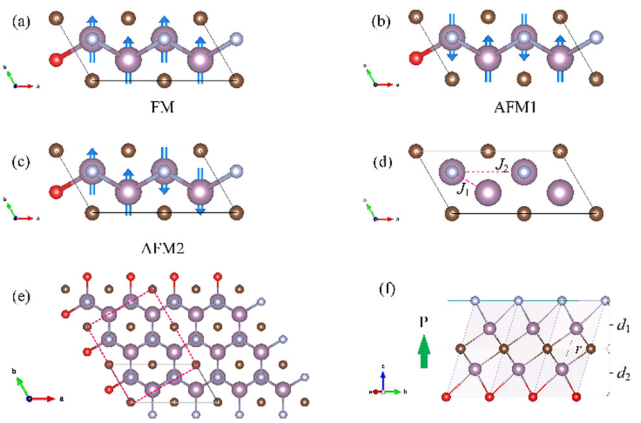

Fig. 5 (a)–(c) Schematics of the three different magnetic orders. (d) J_1 and J_2 denote the nearest-neighbor and next-nearest-neighbor spin exchange paths. (e) and (f) The top view of the Mo_2C-FO supercell; the red dotted lines denote the rectangular lattice chosen for electric polarization calculation. The green arrow represents the direction of electric polarization.

Table 2 The energy difference, exchange integrals of the nearest and next nearest neighbor models, DM parameters, and Curie and Nèel (T_C/T_N) temperatures of the Mo-based MXenes. All energies are in meV

MXenes	$E_{AFM1} - E_{FM}$	$E_{AFM2} - E_{FM}$	J_1	J_2	D	T_C/T_N (K)
Mo_2C-F-O	−641.1	−482.4	−11.01	3.30	−1.61	303
Mo_2C-F-OH	−1580.0	−1069.6	−14.63	3.77	−0.01	321
Mo_2C-O-OH	−664.3	−543.3	−6.15	2.24	−1.17	187
Mo_2C-F_2	−1576.2	−1038.1	−14.59	3.56	−0.02	315
Mo_2C-O_2	−318.8	−180.8	−2.95	0.52	−0.08	69
Mo_2C-$(OH)_2$	−1568.0	−1097.5	−14.52	3.99	−0.05	329

$$E_{AFM2} = -2J_1S_1{\cdot}S_2 - 4J_2S_1{\cdot}S_2$$

where $S_1 = 1$ and $S_2 = 3/2$ correspond to the Mo^{4+} and Mo^{3+} configurations, respectively. The charge disproportionation states modulate the terms $J_{ij}S_iS_j$ such that the local magnetic moments are spatially varying.

In order to simplify the calculations and acquire the potential magnetic properties, we considered S to be the average spin state of all six Mo_2CXX' and ignored local variation in the oxidation states. The calculated exchange interaction parameters of M are listed in Table 2. The positive J_1 and negative J_2 values clearly demonstrate that Mo_2CXX' MXenes prefer the AFM1 magnetic ground state.

To estimate the Curie temperature (T_C) of ferrimagnetic Mo_2C-F-O and Mo_2C-O-OH, and the Nèel temperature of the other four antiferromagnetic materials, Monte Carlo (MC) simulations based on the 2D Heisenberg Hamiltonian model were performed. A 32×32 2D honeycomb lattice and 6.4×10^5 sweep steps were used for all temperatures. T_C/T_N was found using the maximum on the temperature-dependent specific heat and the magnetic susceptibility curve (Fig. 6 and Fig. ESI6, ESI†). The specific heat values were computed as $C_V = (\langle E^2 \rangle - \langle E \rangle^2)/T^2$. From the calculated curve, we found that Mo_2C-F-OH, Mo_2C-F_2, and Mo_2C-$(OH)_2$ owned high T_N of 321, 315, and 329 K, respectively, and ferrimagnetic Mo_2C-F-O and Mo_2C-O-OH had fairly high T_C of 303 K and 187 K, respectively. The non-zero magnetic moment at 0 K reflects the ferrimagnetic behavior of the ground state. There was a positive correlation

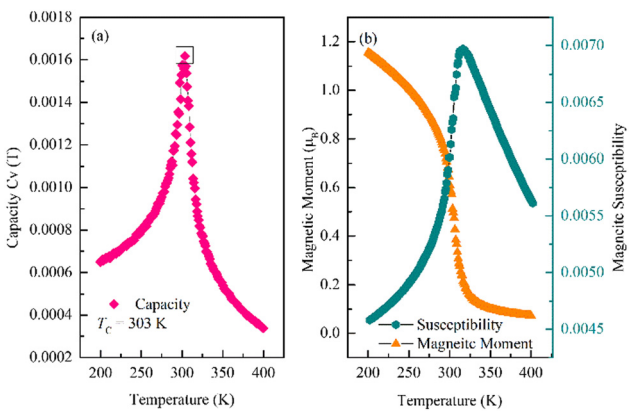

Fig. 6 The results of Monte Carlo simulations. (a) Specific heat C_v of Mo_2C-FO as a function of temperature; (b) magnetic moment and magnetic susceptibility as functions of temperature for Mo_2C-FO.

between T_C/T_N and the nearest-neighbor Mo–Mo bond length (r), as shown in Table 1. The Mo_2CXX' MXenes have higher T_C/T_N than those of CrI_3 (T_C = 45 K) and $Cr_2Ge_2Te_6$ (T_C = 30 K), suggesting application potential in nano-spintronic devices.

C. Out-of-plane polarization and magnetoelectric coupling effect in the asymmetric Janus Mo-based MXenes

As mentioned above, the lack of an inversion center and mirror symmetry in the asymmetric Janus structures leads to a finite out-of-plane polarization.[46–48] Due to the difference in electronegativity between the terminal atoms, the charge is transferred from the metal layer to the terminal atoms; this phenomenon together with the difference in finite displacement along the c direction creates an out-of-plane dipole moment. The magnitude of the out-of-plane dipole moment was calculated based on the movement in the vacuum level on the two sides of the terminal layer, as shown in Fig. 7. We could see that due to the dipole-induced potential step, the vacuum levels on the two sides of the monolayer were, in general, different in the asymmetric Janus MXenes. However, there was no potential step in the symmetric Mo_2C-F_2, Mo_2C-O_2, and Mo_2C-$(OH)_2$. The work function, which is the difference between the vacuum energy level and the Fermi energy level, is listed in Table S3 (ESI†).

From the results of the averaged electrostatic potential, the asymmetric Janus monolayer Mn_2C-FO, Mo_2C-FOH, and Mo_2C-O-OH can be considered potential magnetoelectric materials. The electric polarizations were calculated by using the Berry phase method. Taking Mo_2C-FO as an example, we first determined a central symmetric structure as a reference, as shown in Fig. 8(a) (inset: middle). The central symmetric structure was composed of out-of-plane terminal ordered atoms (similar to o-MXenes in the literature[48]). In this work, we defined the out-of-plane ordered structure as the O-phase. The structure of the O-phase could be viewed as the ordered flipping of the terminal atom of the asymmetric Janus structure (J-,J'-phase), as seen in the Fig. 8(a) inset. The O-phase possessed the inversion center at ($-x$, $-y$, $-z$) and belonged to the space group $P2_1/m$. The

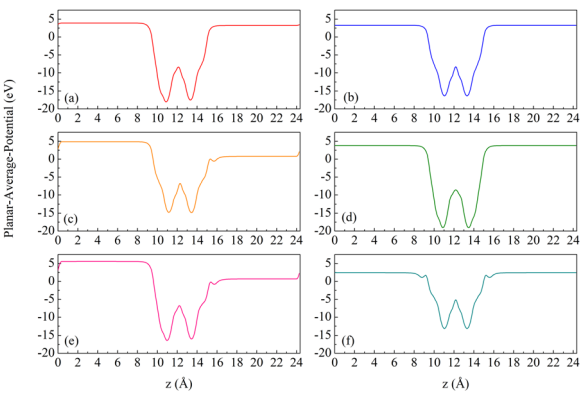

Fig. 7 The averaged electrostatic potential *vs.* the vacuum level for (a) Mn_2C-FO; (b) Mo_2CF_2; (c) Mo_2C-FOH; (d) Mo_2C-O_2; (e) Mo_2C-O-OH; and (f) Mo_2C-$(OH)_2$. One step in the potential is observed due to the out-of-plane dipole moment in asymmetric Janus MXenes.

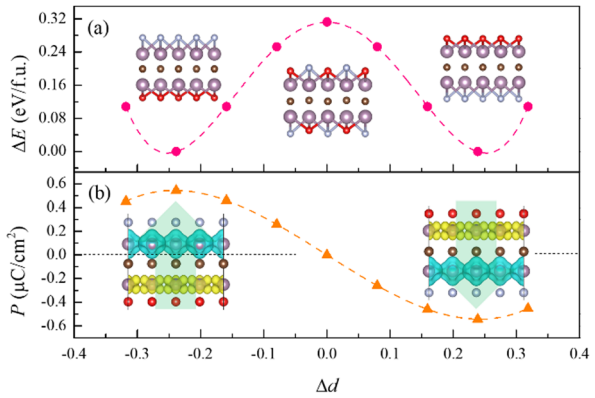

Fig. 8 (a) Total energy as a function of the difference in layer distance Δd (as defined in Fig. 5(f)). Inset: The J-, O-, J'-phases of Mo2C-FO. (b) Electric polarization as a function of Δd. Inset: Cyan and yellow represent the spin-polarized charge densities of the spin-up and spin-down channels, respectively. The green arrows mark the direction of electric polarization.

breaking of vertical-mirror and inversion symmetries in the J-phase Mo_2C-FO (belonging to the $P3m1$ space group) led to out-of-plane electric polarization. As shown in Fig. 8(a), there were two degenerate J-phases with differences in layer distance $\Delta d < 0$ and $\Delta d > 0$, which passed through a saddle point (the O-phase with $\Delta d = 0$) in a double-well potential curve. These two phases could convert to each other by terminal atom flipping, as seen in Fig. ESI7 (ESI†). The electric polarization induced by the asymmetric Janus structure for the J- and J'-phases were of opposite sign (Fig. 8(b)) but the same in magnitude (about 0.55 μC cm^{-2}).

We designed a possible switching path for reversing the FE polarization of Mo_2C-FO. As shown in Fig. ESI7 (ESI†), the polarization was switched from +P to −P through progressive flipping of the F–O pairs. Simultaneously, the symmetry changed from the original J-phase $P3m1$ to low symmetry Pm, then to central symmetry $P2_1/m$, and finally to J'-phase $P3m1$, confirming the reversal of electric polarization. Interestingly, the vertical spatial distribution of the spin magnetic moments could be tuned by the reversal of the out-of-plane electric polarization. This suggests that the interlayer ferrimagnetic orders can be switched by reversing electric polarization *via* applying an electric field and thereby realizing magnetoelectric coupling. It is worth noting that this coupling mechanism is not suitable for the Mo_2C-F-OH and Mo_2C-O-OH asymmetric systems, because their J- and J'-phases were not low-energy structures, as seen in Fig. ESI7 (ESI†). It will be interesting to investigate whether these systems are experimentally realizable and evaluate the polarization switching characteristics.

4. Conclusions

We have demonstrated that asymmetric Janus Mo_2CXX' are ideal 2D multifunctional materials, in which intrinsic ferrimagnetism and switchable out-of-plane polarization can co-exist, by DFT+U calculations. From the AIMD and phonon spectrum

calculations, the thermal and dynamic stability of six functionalized Mo_2C were identified. The magnetic phase-transition temperatures were determined by Monte Carlo simulations. A fair high T_C of 303 K has been calculated for Mo_2C-FO. Our DFT+U calculation results also provide a mechanism of magnetoelectric coupling, in which the reversal of electric polarization is driven by terminal-layer atom-pair flipping. Our work expands the opportunities for the application of the monolayer MXene Mo_2C, establishes a model to engineer switchable electric polarization in 2D, and discovers a class of 2D materials with switchable out-of-plane polarization, with implications for next-generation nano-spintronic devices.

Author contributions

C. X.: conceptualization, and writing – original draft, Z. F. and Z. S.: data curation, software, H. L. and G. J.: formal analysis, and supervision, F. P. and Y. S.: investigation.

Conflicts of interest

There are no conflicts to declare.

Acknowledgements

This work was supported by the National Natural Science Foundation of China (No. 12004051), Jilin Province Science and Technology Association Project (No. QT202110), and Soft Science Research Project of Guangdong Province (No. 2017B030301013). We thank the High Performance Computing Center of School of Advanced Materials, Peking University Shenzhen Graduate School for calculation resource.

Notes and references

1 S. W. Cheong and M. Mostovoy, *Nat. Mater.*, 2007, **6**, 13–20.
2 N. A. Spaldin and M. Fiebig, *Science*, 2005, **309**, 391–392.
3 T. Kimura, T. Goto, H. Shintani, K. Ishizaka, T. Arima and Y. Tokura, *Nature*, 2003, **426**, 55–58.
4 H. Katsura, N. Nagaosa and A. V. Balatsky, *Phys. Rev. Lett.*, 2005, **95**, 057205.
5 C. Ederer and N. A. Spaldin, *Phys. Rev. B: Condens. Matter Mater. Phys.*, 2005, **71**, 060401.
6 C. Xin, B. Q. Song, Z. X. Sun, Z. X. Hu, B. S. Yuan, H. Li, G. Y. Jin and F. Pan, *Appl. Phys. Lett.*, 2020, **116**, 242901.
7 M. L. Xu, C. X. Huang, Y. W. Li, S. Y. Liu, X. Zhong, P. Jena, E. J. Kan and Y. C. Wang, *Phys. Rev. Lett.*, 2020, **124**, 067602.
8 M. Wu, J. D. Burton, E. Y. Tsymbal, X. C. Zeng and P. Jena, *Phys. Rev. B: Condens. Matter Mater. Phys.*, 2013, **87**, 081406.
9 C. Xin, J. X. Zheng, Y. T. Su, S. K. Li, B. K. Zhang, Y. C. Feng and F. Pan, *J. Phys. Chem. C*, 2016, **120**, 22663–22669.
10 S. N. Shirodkar and U. V. Waghmare, *Phys. Rev. Lett.*, 2014, **112**, 157601.
11 A. Chandrasekaran, A. Mishra and A. K. Singh, *Nano Lett.*, 2017, **17**, 3290–3296.
12 R. X. Fei, W. Kang and L. Yang, *Phys. Rev. Lett.*, 2016, **117**, 097601.
13 F. C. Liu, J. L. Wang and Z. Liu, *et al.*, *Nat. Commun.*, 2016, **7**, 12357.
14 K. Chang, X. Chen and S. H. Ji, *et al.*, *Science*, 2016, **353**, 274–278.
15 B. Huang, J. H. Pablo and X. D. Xu, *et al.*, *Nature*, 2017, **546**, 270.
16 C. Gong, L. Li, Z. Li, H. Ji, A. Stern, Y. Xia, T. Cao, W. Bao, C. Wang, Y. Wang, Z. Q. Qiu, R. J. Cava, S. G. Louie, J. Xia and X. Zhang, *Nature*, 2017, **546**, 265.
17 Y. Y. Liu, W. Zhou, G. Tang, C. Yang, X. Y. Wang and J. W. Hong, *J. Phys. Chem. C*, 2019, **123**, 28919–28924.
18 M. H. Wu, *ACS Nano*, 2021, **15**, 9229–9237.
19 W. Sun, W. X. Wang, H. Li, G. B. Zhang, D. Chen, J. L. Wang and Z. X. Cheng, *Nat. Commun.*, 2020, **11**, 5930.
20 C. M. Zhang, Y. H. Nie, S. Sanvito and A. J. Du, *Nano Lett.*, 2019, **19**, 1366–1370.
21 Z. N. Sun, X. R. Li, J. W. Li, Y. D. Wei, H. Guo and J. Wang, *npj 2D Mater. Appl.*, 2022, **6**, 69.
22 N. Michael, N. M. Vadym, W. B. Michel and Y. Gogotsi, *Adv. Mater.*, 2014, **26**, 992–1005.
23 A. VahidMohammadi, J. Rosen and Y. Gogotsi, *Science*, 2021, **372**, 1165.
24 M. M. Hasan, M. M. Hossain and H. K. Chowdhury, *J. Mater. Chem. A*, 2021, **9**, 3231–3269.
25 Y. T. Guo, S. Jin, L. B. Wang, P. G. He, Q. K. Hu, L. Z. Fan and A. G. Zhou, *Ceram. Int.*, 2020, **46**, 19550–19556.
26 C. Si, J. Zhou and Z. M. Sun, *ACS Appl. Mater. Interfaces*, 2015, **7**, 17510–17515.
27 N. C. Frey, A. Bandyopadhyay, H. Kumar, B. Anasori and Y. Gogotsi, *ACS Nano*, 2019, **13**, 2831–2839.
28 J. J. Zhang, L. Lin, Y. Zhang, M. Wu, B. I. Yakobson and S. Dong, *J. Am. Chem. Soc.*, 2018, **140**, 9768–9773.
29 C. Huang, J. Zhou, H. Sun, F. Wu, Y. Hou and E. Kan, *Nano Lett.*, 2022, **13**, 5191–5197.
30 B. Anasori, M. R. Lukatskaya and Y. Gogotsi, *Nat. Rev. Mater.*, 2017, **2**, 16098.
31 G. Kresse and J. Hafner, *Phys. Rev. B: Condens. Matter Mater. Phys.*, 1993, **47**, 558.
32 G. Kresse and J. Furthmüller, *Phys. Rev. B: Condens. Matter Mater. Phys.*, 1996, **54**, 11169.
33 P. E. Blöchl, *Phys. Rev. B: Condens. Matter Mater. Phys.*, 1994, **50**, 17953.
34 A. Tkatchenko and M. Scheffler, *Phys. Rev. Lett.*, 2009, **102**, 073005.
35 S. L. Dudarev, G. A. Botton, Y. Y. Savrasov, C. J. Humphreys and A. P. Sutton, *Phys. Rev. B: Condens. Matter Mater. Phys.*, 1998, **57**, 1505.
36 H. J. Monkhorst and J. D. Pack, *Phys. Rev. B: Condens. Matter Mater. Phys.*, 1976, **13**, 5188.
37 P. Pulay, *Chem. Phys. Lett.*, 1980, **73**, 393–398.
38 R. D. King-Smith and D. Vanderbilt, *Phys. Rev. B: Condens. Matter Mater. Phys.*, 1993, **47**, 1651.
39 A. Savin, R. Nesper, S. Wengert and T. F. A. Fässler, *Angew. Chem., Int. Ed. Engl.*, 1997, **36**, 1808–1832.

40 K. Momma and F. Izumi, *J. Appl. Crystallogr.*, 2011, **44**, 1272–1276.
41 H. M. Weng, A. Ranjbar, Y. L. Liang, Z. D. Song, M. Khazaei, S. J. Yunoki, M. Arai, Y. Kawazoe, Z. Fang and X. Dai, *Phys. Rev. B: Condens. Matter Mater. Phys.*, 2015, **92**, 075436.
42 S. Baroni, S. de Gironcoli, A. Dal Corsoo and P. Giannozzi, *Rev. Mod. Phys.*, 2001, **73**, 515.
43 J. He, P. Zhou, N. Jiao, S. Y. Ma, K. W. Zhang, R. Z. Wang and L. Z. Sun, *Sci. Rep.*, 2014, **4**, 4014.
44 H. Jin, Y. Dai, B. Huang and M. H. Whangbo, *Appl. Phys. Lett.*, 2009, **94**, 162505.
45 J. J. He, P. Lyu, L. Z. Sun, A. M. Garcia and P. Nachtigall, *J. Mater. Chem. C*, 2016, **4**, 6500–6509.
46 Z. Y. Guan and S. Ni, *ACS Appl. Mater. Interfaces*, 2020, **12**, 53067–53075.
47 Z. Y. Guan, S. Ni and S. L. Hu, *J. Phys. Chem. C*, 2018, **122**, 6209–6216.
48 Z. Y. Guan and S. Ni, *ACS Appl. Electron. Mater.*, 2021, **3**, 3147–3157.